Geophysical Research Letters

RESEARCH LETTER
10.1029/2020GL089395

Intensification of Westerly Wind Bursts Caused by the Coupling of the Madden-Julian Oscillation to SST During El Niño Onset and Development

Yu Liang[1], Alexey V. Fedorov[1,2], and Patrick Haertel[1]

[1]Department of Earth and Planetary Sciences, Yale University, New Haven, CT, USA, [2]LOCEAN/IPSL, Sorbonne University, Paris, France

Key Points:

- The Madden-Julian Oscillation convective envelope shifts from the southern hemisphere toward the equator during El Niño onset
- The Madden-Julian Oscillation strengthens in the central equatorial Pacific, but weakens in the northwestern Pacific during El Niño development
- Westerly wind bursts are strongly enhanced due to the coupling between the Madden-Julian Oscillation and sea surface temperature anomalies

Supporting Information:

Supporting Information may be found in the online version of this article.

Correspondence to:

Y. Liang,
yu.liang@yale.edu

Citation:

Liang, Y., Fedorov, A. V., & Haertel, P. (2021). Intensification of westerly wind bursts caused by the coupling of the Madden-Julian Oscillation to SST during El Niño onset and development. *Geophysical Research Letters*, *48*, e2020GL089395. https://doi.org/10.1029/2020GL089395

Received 18 JUN 2020
Accepted 28 SEP 2020

Abstract The Madden-Julian Oscillation (MJO) plays an important role in El Niño dynamics in connection with westerly wind bursts (WWBs) that occur in the equatorial Pacific; however, our understanding of the relationship between these climate phenomena remains incomplete. Here, we use a Lagrangian Atmospheric Model (LAM) to examine the response of the MJO and resulting WWBs to sea surface temperature (SST) anomalies similar to those observed during the onset and development of El Niño. We find that when a localized SST anomaly (≤1°C) is imposed in the western-central equatorial Pacific between December and April (mimicking El Niño onset), the MJO convective envelope shifts from the southern hemisphere toward the equator. When an SST anomaly (≤1.5°C) is imposed in the central-eastern equatorial Pacific between May and November (mimicking El Niño development), the MJO weakens in the northwestern Pacific, but strengthens in the central equatorial Pacific. In both experiments, the ensuing changes enhance MJO activity along the equator, facilitating WWBs.

Plain Language Summary The Madden-Julian Oscillation (MJO) is an eastward propagating planetary-scale envelope of clouds, heavy rainfall, and winds in the tropical atmosphere. It can contribute to the development of El Niño through the generation of westerly wind bursts (WWBs). El Niño is marked by anomalously warm sea surface temperature (SST) in the central and eastern equatorial Pacific, which has profound impacts on global weather patterns. WWBs are episodic bursts of strong westerly winds in the western-central equatorial Pacific lasting several weeks and usually observed during the onset (spring) and development (summer) stages of El Niño. As WWBs contribute to the growth of El Niño and affect its predictability, it is important to understand the mechanisms of WWBs. In this study, we use a novel numerical model to investigate how WWBs are generated by the MJO and how this process is affected by El Niño-related SST anomalies. We find that during the onset (development) stages of El Niño, positive SST anomalies in the western (central-eastern) equatorial Pacific draw the MJO-induced precipitation anomalies toward the equator, facilitating WWB generation. We also find that stronger MJO events tend to generate more intense WWBs. Our results can help improve the prediction of WWBs critical to El Niño development.

1. Introduction

The dominant intraseasonal mode of variability in the tropical atmosphere, the Madden-Julian Oscillation (MJO) is characterized by planetary-scale eastward propagating disturbances in atmospheric convection, winds, and cloud cover (e.g., Madden & Julian, 1972; Wheeler & Kiladis, 1999). The MJO shows a strong seasonality—in boreal winter it is strongest in the southern hemisphere, while in boreal summer it is strongest north of the equator (Zhang & Dong, 2004). The MJO affects major tropical weather systems, including the Asian and Australian monsoons (e.g., Hendon & Liebmann, 1990; Lau & Chan, 1986), as well as tropical cyclogenesis (e.g., Liebmann et al., 1994).

Many studies have investigated the relationship of the MJO with the El Niño-Southern Oscillation (ENSO)—the dominant interannual climate mode in the tropics. Overall, the indices describing MJO activity appear to be uncorrelated with ENSO, which suggests that the MJO interannual variability is mostly internally generated (Hendon et al., 1999; Slingo et al., 1999). However, an enhanced MJO activity over the western equatorial Pacific (represented by filtered winds and outgoing longwave radiation (OLR) averaged within 5°N–5°S) is often observed in the boreal spring of El Niño years (Hendon et al., 2007). An eastward

extension of the MJO convective envelope has also been noted during the development of El Niño (Hendon et al., 1999; Kessler, 2001), and several models of ENSO-MJO interaction have been proposed (Kessler et al., 1995; Kessler & Kleeman, 2000).

With the increasing occurrence of the so-called Central Pacific (CP) El Niño after the year 2000 (e.g., Ashok et al., 2007; Capotondi et al., 2015; Hu & Fedorov, 2018; Kao & Yu, 2009; Kug et al., 2009; Yeh et al., 2009), some studies investigated different responses of the MJO to CP and eastern Pacific (EP) El Niño types, which are defined by different shapes of sea surface temperature (SST) anomalies (e.g., Chen et al., 2016; Gushchina & Dewitte, 2012). However, most of these studies diagnosed MJO activity using MJO-filtered and equatorially averaged indices, for surface zonal winds and OLR in particular, but ignored changes in the MJO horizontal structure, especially off the equator.

The generation of westerly wind bursts (WWBs) by the MJO provides another link to ENSO. WWBs are episodic strong westerly winds in the western and central equatorial Pacific, usually lasting up to several weeks and frequently observed during the onset and development stages of El Niño (e.g., Hartten, 1996; Vecchi & Harrison, 2000, or recently; Liang & Fedorov, 2021). WWBs excite downwelling oceanic Kelvin waves depressing the equatorial thermocline in the EP and at the same time transporting surface warm water eastward, often contributing to the development of El Niño (Fedorov, 2002; Fedorov et al, 2003, 2015; Hu et al., 2014; Hu & Fedorov, 2019; Lengaigne et al. 2002; McPhaden & Yu, 1999; Yu & Fedorov, 2020). A large fraction of WWBs are generated within the MJO and in particular by tropical cyclones embedded in the MJO (Lian et al., 2018; Liang & Fedorov, 2021; Puy et al., 2016; Seiki & Takayabu, 2007).

The connection between WWBs, the MJO, and ENSO remains under debate. Although some studies suggested that a strong MJO could favor more frequent and stronger WWBs, this does not preclude the dependence of WWBs on SST (Puy et al., 2016; Seiki & Takayabu, 2007). Furthermore, because the MJO varies seasonally (Zhang & Dong, 2004) and El Niño is phase locked to the annual cycle (e.g., Hirst, 1986; Neelin et al., 2000; Rasmusson & Carpenter, 1982), the relationship between El Niño, the MJO and WWBs can vary as a function of the season.

Recently, using atmospheric reanalysis data, Liang and Fedorov (2021) applied a composite analysis and identified favorable background conditions in the equatorial region that could enhance WWB generation by modifying the MJO horizontal structure during the onset and development stages of El Niño. Specifically, they have described warm equatorial SST anomalies and the corresponding wind anomalies that emerge in winter and summer (Figures 1a and 1b) and facilitate WWB generation presumably by shifting the MJO's convective activity, including tropical cyclones, toward the equator and eastward. Here, our goal is to explore, by means of idealized numerical experiments, how such background SST anomalies would affect the MJO and WWB generation.

2. Methods

Our main tool is the Lagrangian Atmospheric Model (LAM), which is a full GCM that represents the atmosphere as a collection of conforming air parcels whose motions are predicted by Newtonian mechanics (Haertel et al. 2014). Its vertical resolution is approximately 31 hPa and the equivalent Eulerian horizontal resolution is approximately 1° on the equator (coarser poleward). The time step of integration is 15 min with the output saved every 6 h. The main advantage of LAM is its realistic and robust simulation of the MJO and WWBs at this relatively coarse model resolution (Haertel, 2012, 2018, 2020; Haertel et al., 2014, 2015, 2017). More conventional, Eulerian GCMs often struggle to properly simulate the MJO, and even state-of-the-art models do not necessarily capture the full amplitude and eastward propagation of the MJO (e.g., Hung et al., 2013). In contrast, the Lagrangian approach is well suited for simulating the MJO as (a) it reproduces the observed sensitivity of convective divergence profiles to atmospheric stratification, which is important for the MJO's mechanism of building up moisture on its leading edge (Haertel et al. 2008) and (b) it can model moisture transport with zero numerical diffusion, hence maintaining tight moisture gradients, including the eastward moisture transport by the MJO's equatorial westerly wind anomalies (Haertel et al. 2017).

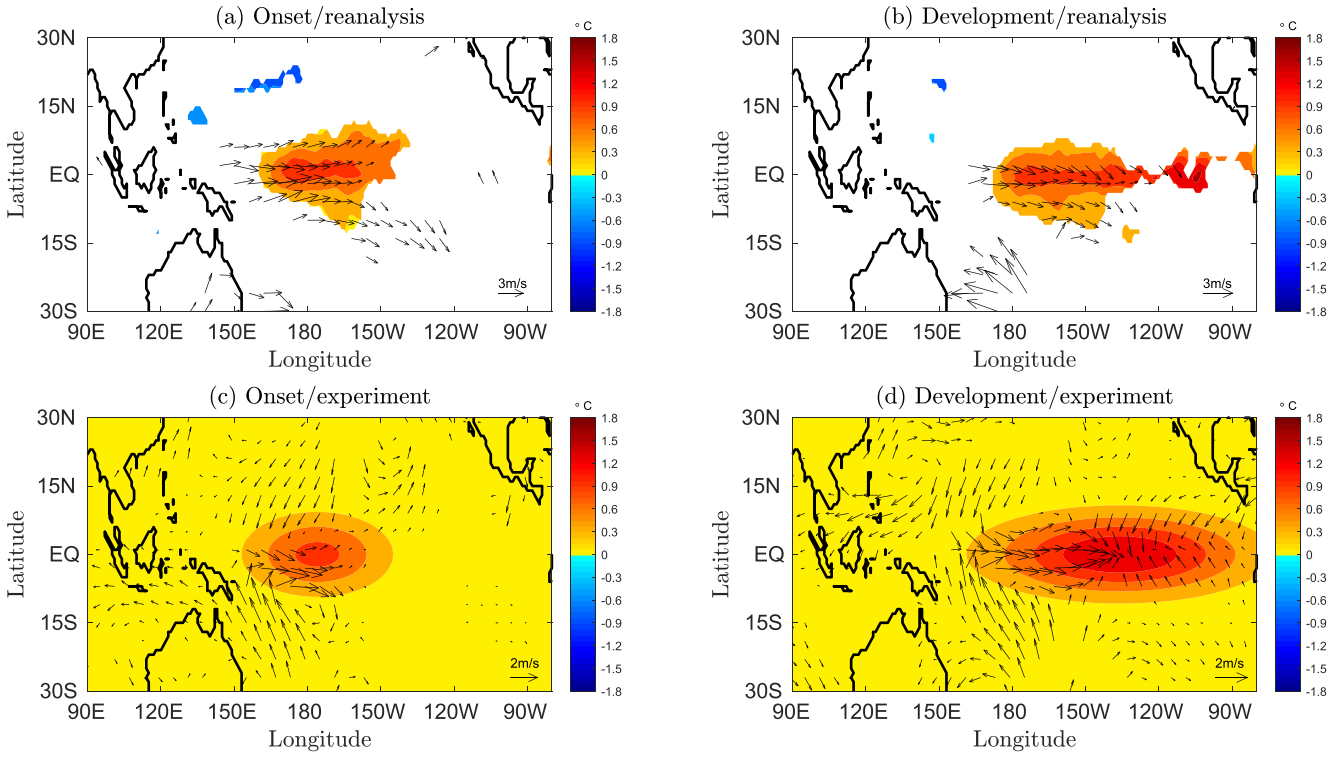

Figure 1. (a) Winter-spring (DJFMA) and (b) summer-fall (MJJASON) composites for environmental SST and 1,000 hPa surface wind differences between the observed wMJO and nwMJO (defined in the text after Liang & Fedorov [2021]). The differences can be interpreted as background SST and surface wind anomalies during the onset and development stages of El Niño that favor WWB generation. Color shading denotes SST anomalies (in °C) that are statistically significant at a 95% confidence level; likewise, wind vectors (in m/s) are shown if the zonal component meets the 95% significance level. (c) Winter-spring (DJFMA) and (d) summer-fall (MJJASON) idealized Gaussian-shape SST anomalies (color, °C) added to the perturbation experiments to mimic the observed SST anomalies. Also shown are 1,000 hPa wind anomalies, relative to the control experiment, induced by the imposed SST forcing. Wind vectors are shown if the zonal component meets the 95% significance level. SST, sea surface temperature; WWB, westerly wind burst.

LAM also reproduces a fairly realistic mean state (Haertel et al. 2014), especially the background westerlies in the western equatorial Pacific, which may be important for WWB generation while missing in some general circulation models (Seiki et al., 2011). One known bias of LAM is a too strong MJO amplitude on the equator near the dateline, where the observed MJO usually starts to decay (e.g., Figure 8 of Wheeler and Hendon 2004). Also, the modeled MJO dominates intraseasonal oscillations in the model while other equatorial waves remain relatively weak. Finally, the wind response to tropical SST anomalies in LAM is slightly weaker than the observations (Figure 1).

Because LAM diagnoses circulation by tracing individual parcels, for the convenience of analysis, we interpolate the wind and precipitation fields on 2° longitude × 2° latitude and 4° longitude × 4° latitude grids, respectively. The structure of the model's MJO is shown in Figures S1 and S2. To isolate the MJO signal, wind velocities at 1,000 hPa and precipitation are filtered to retain only eastward propagating signals with zonal wave numbers 1–5 and periods of 30–95 days (Wheeler and Kiladis, 1999).

WWBs are computed from daily U1000 hPa anomalies, calculated relative to the 5-day running-mean daily climatology of the Control experiment (defined below) following Liang and Fedorov (2021). WWBs are identified if three criteria are met: (a) U1000 hPa anomalies averaged between 2°N and 2°S are stronger than a 5 m/s threshold. (b) The area that satisfies the criterion 1 has a zonal extent of at least 10° of longitude. (c) The first two criteria are met for 5 days or longer. In addition, we apply a criterion for merging two WWBs: (d) if two WWBs are separated by less than 3° of longitude and 3 days, they are considered as one WWB.

To measure the strength of WWBs, we define Amp_{WWB} for each WWB by integrating equatorially averaged U1000 hPa anomalies over longitude and time (Equation 1).

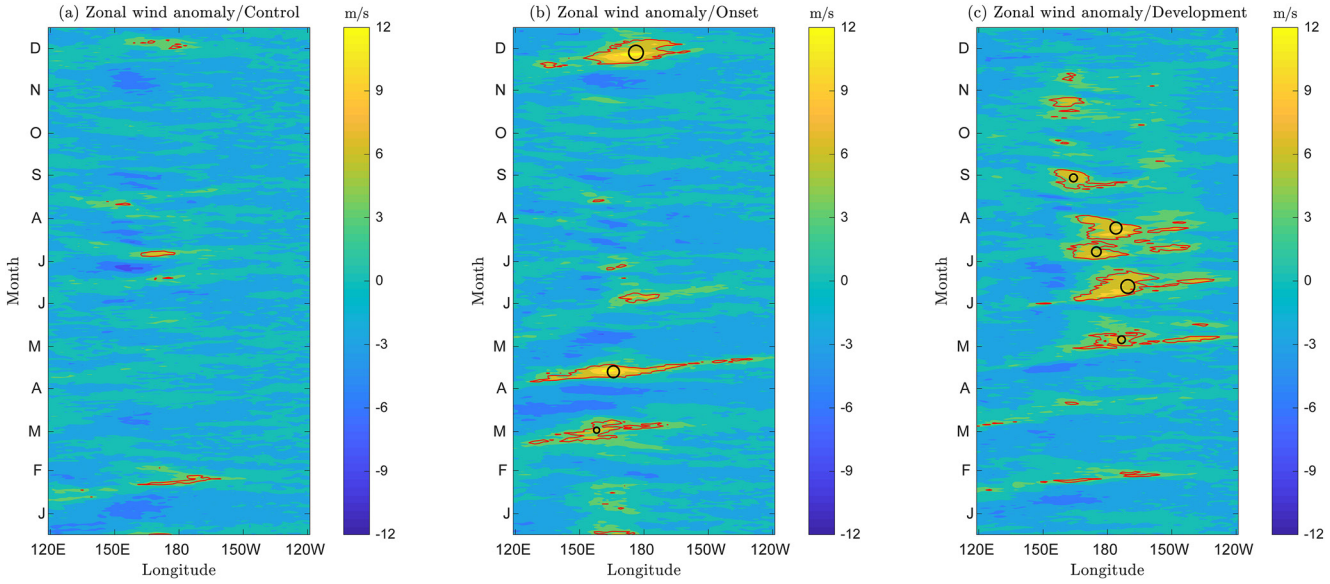

Figure 2. Examples of simulated zonal wind anomalies in the (a) Control, (b) Onset, and (c) Development experiments. Zonal wind anomalies are calculated relative to the model 5-day running-mean daily climatology and averaged between 2°N and 2°S. Red contours indicate values exceeding the 5 m/s threshold; WWBs are marked with black circles with their radii proportional to Amp_{WWB}. WWB, westerly wind burst.

$$Amp_{WWB} = \int_{lon\,t}\int U1000hPa_{ano}\left(x,t\right)dxdt \tag{1}$$

$$day_0 = \frac{\int_{lon\,t}\int U1000hPa_{ano}\left(x,t\right)day\left(t\right)dxdt}{Amp_{WWB}} \tag{2}$$

$$lon_0 = \frac{\int_{lon} U1000hPa_{ano}\left(x,day_0\right)lon\left(x\right)dx}{\int_{lon} U1000hPa_{ano}\left(x,day_0\right)dx} \tag{3}$$

The central date day_0 of each WWB is defined by a weighted date average given by Equation 2. Similarly, we define the central longitude lon_0 on day_0 using Equation 3. In Figure 2 examples of simulated WWBs are marked with black circles centered on lon_0 and day_0; the radius of each circle is proportional to Amp_{WWB}.

As WWBs are preferentially generated within the westerly phase of the MJO in the western-central equatorial Pacific (Puy et al., 2016; Seiki & Takayabu, 2007), we define the date when westerly wind anomalies of the MJO averaged between 120°E and 180°E, 15°N and 15°S reach their maximum as $day_{westerly}$. Similarly, we define the MJO amplitude (Amp_{MJO}) as the maximum filtered precipitation averaged in the same region. The MJO amplitude could also be defined from zonal wind anomalies, but our results would not be affected. Further, MJO events are divided into two types: WWB-generating MJO events (wMJO) if there occurs a WWB within westerly wind anomalies of the MJO; and non-WWB-generating MJO events (nwMJO).

Following Liang and Fedorov (2021), to obtain background SST and wind anomalies favorable for WWB generation during the onset and development stages of El Niño (Figures 1a and 1b), we subtract the composite environmental SST and wind fields of the nwMJO from the wMJO, using the ERA-interim reanalysis (Dee et al., 2011). The differences can be interpreted as the observed background conditions that facilitate WWB generation. The SST anomalies are crudely approximated by idealized Gaussian expressions (Equations 4 and 5) and then used in the perturbation experiments.

We conduct three sets of experiments with LAM, including the Control experiment and two experiments mimicking the onset and development stages of El Niño. Each experiment has six ensemble members, and

each ensemble member is integrated for 3 years. The Control experiment is forced by monthly climatological SST averaged for 1990–2010. In the El Niño onset experiment (hereafter the Onset experiment), a Gaussian-shaped positive SST anomaly is added to the western-central equatorial Pacific from December to April (extended winter season). In the El Niño development experiment (the Development experiment), a Gaussian-shaped positive SST anomaly is added to the central-eastern equatorial Pacific from May to November (extended summer season). The imposed SST anomalies (Figures 1c and 1d) are computed as follows:

$$SST_{onset} = 1°C * exp\left(-\left(longitude - 185°\right)^2 / 2 / 20°^2\right) * exp\left(-latitude^2 / 2 / 6°^2\right) \quad (4)$$

$$SST_{develop} = 1.5°C * exp\left(-\left(longitude - 225°\right)^2 / 2 / 35°^2\right) * exp\left(-latitude^2 / 2 / 6°^2\right) \quad (5)$$

The selected parameters allow us to mimic the observed SST anomalies (Figures 1a and 1b). Further, patches of westerly wind anomalies (~2 m/s) develop to the west of the imposed SST anomalies, following a classical Gill-type response (Gill, 1980; Matsuno, 1966); they are comparable to the observed wind composites. Finally, six top MJO events are selected from each ensemble member in the Control and Onset experiments based on Amp_{MJO} during the extended winter; and six top MJO events are selected from each ensemble member in the Control and Development experiments during the extended summer. In other words, on average two MJO events are selected per season per year.

Note that while we refer to the perturbation experiments as the El Niño Onset and Development, they are atmospheric experiments without any dynamical ocean-atmosphere coupling. Previous studies show that the coupling between WWBs and SST (e.g., Lengaigne et al. 2003; Vecchi & Harrison, 2000) and between the MJO and SST (Kessler & Kleeman, 2000) could further amplify warm SST anomalies along the equator and strengthen the following WWBs.

3. Results

In this study, we focus on the response of the MJO to equatorial SST anomalies as related to WWB generation and therefore we consider the model's MJO composites on $day_{westerly}$, that is, around the maximum strength of westerly winds. These composites generally correspond to Phase 6 of the conventional Real-time Multivariate (RMM) MJO index (Wheeler and Hendon, 2004).

First, we compare composites for the top 36 MJO events in the Control and Onset experiments during the extended winter (precipitation and surface winds are shown in Figures 3a and 3b). The winter MJO in these experiments shares a number of general features: for example, positive precipitation and westerly wind anomalies are mainly confined to the southern hemisphere, with westerly wind anomalies prevailing through the precipitation anomalies.

Compared to the MJO in the Control experiment, the Onset experiment shows the enhancement of positive precipitation and westerly wind anomalies on the equator, and a reduction off the equator. The difference between the two (Onset minus Control) has a northeast-southwest dipole structure (Figure 3c) indicating that the imposed SST anomaly in the western-central equatorial Pacific draws the MJO convective activity toward the equator. As the MJO amplitudes in the Control and Onset experiments remain comparable (Figures S3a and S3b), the enhancement of MJO activity in the equatorial band in boreal spring (also present in the observations by Hendon et al. [2007]) is mainly caused by the change to the MJO horizontal structure. As a result, the generation of WWBs along the equator is greatly enhanced.

In the Control experiment, only five WWBs are generated during the extended winter across all 18 years of the simulations (Figure 4a), that is, fewer than 0.5 wind burst per winter season on average. Among the five WWBs, four are generated by four individual MJO events. In contrast, in the Onset experiment 27 WWBs are generated (~1.5 bursts per winter season), among which 18 are generated by the MJO, and they are much stronger (Figure 4b). This is consistent with previous findings that the eastward expansion of the warm pool is favorable for WWB generation (e.g., Eisenman et al., 2005; Fedorov et al. 2015; Gebbie et al., 2007; Gebbie and Zipterman, 2009; Hu et al., 2014; Hu & Fedorov, 2019; Tziperman & Yu, 2007).

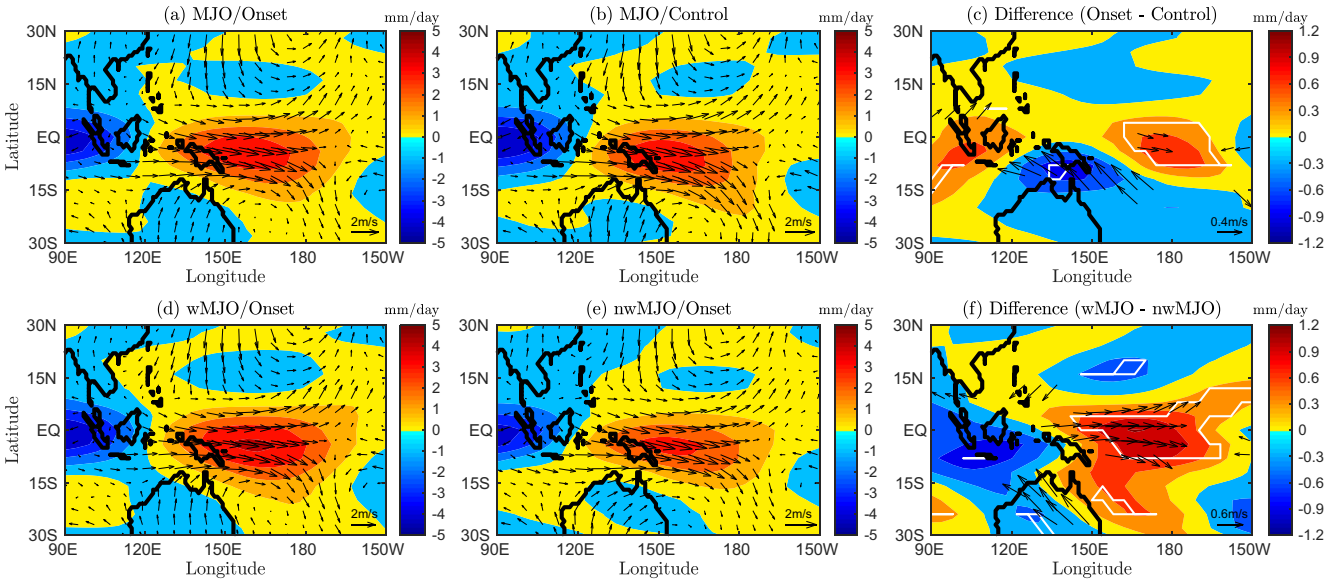

Figure 3. Composites of space-time filtered precipitation and 1,000 hPa wind fields for the strongest MJO events simulated between December and April in (a) the Onset and (b) Control experiments (36 events are selected in each experiment), and (c) their difference (left panel minus middle panel). Space-time filtering (zonal wavenumbers 1–5, periods 30–95 days) has been applied to retain eastward-propagating signals. Color shading denotes precipitation anomalies and black arrows indicate surface wind anomalies. In panel (c) white contours mark statistically significant regions with a 95% confidence level, and wind difference is shown if zonal wind component is statistically significant at the same 95% level. (d)–(f) As in the top row but for 18 wMJO events and 18 nwMJO events identified among the 36 MJO events of the Onset experiment. The warm SST anomaly imposed in the Onset experiment intensifies MJO activity along the equator, which is critical for WWB generation. MJO, Madden-Julian Oscillation.

We stress that in the Control experiment a few WWBs are still generated, suggesting that WWBs can develop under neutral conditions (within the MJO or possibly due to cold surges from mid-latitudes, Chu, 1988). Also, the number and amplitude of generated WWBs in the Onset experiment vary greatly across ensemble members (Figure S4b). Thus, even in the presence of a positive SST anomaly, WWB generation is not guaranteed. In fact, out of the top 36 MJO events in the Onset experiment, only a half are wMJO events.

It is instructive to compare the composites of wMJO and nwMJO events in the Onset experiment, as their horizontal structures are fairly similar (Figures 3d and 3e). Subtracting the nwMJO composite from the wMJO, we see an enhancement of positive precipitation and westerly wind anomalies along the equator but no reduction off the equator (Figure 3f), which indicates that the main difference between the wMJO and nwMJO is the event amplitude. Note that wind anomalies south of 15°S are related to extratropical waves, and not to the MJO (e.g., Andersen & Kuang, 2012). These results suggest that even though positive background SST anomalies are favorable for WWB generation as they draw MJO convective activity toward the equator, only MJO events of sufficiently large amplitudes can generate WWBs (consistent with Seiki & Takayabu [2007]). Therefore, it is both background conditions and internal variability that control WWB generation.

Figure S5 shows several snapshots of a wMJO event—the one that caused the second WWB seen in Figure 2b. This burst is generated by westerly wind anomalies of this propagating wMJO and further amplified by a tropical cyclone developing within the convective phase of the event, which is consistent with the findings in Liang and Fedorov (2021) who stressed the role of tropical cyclones embedded in the MJO for WWB generation.

Next, we examine the response of the MJO to anomalous SST emerging during the development of El Niño. Figures 5a and 5b compare the composites of space-time filtered precipitation and surface winds for the top 36 MJO events during the extended summer computed on $day_{westerly}$ for the Development and Control experiments. In the Control experiment, we find two centers of positive precipitation anomalies with prevailing westerly wind anomalies (Figure 5b), one in the north western Pacific and the other in the central equatorial Pacific, which resemble the horizontal structure of the Phase 6 May–June composite of the MJO

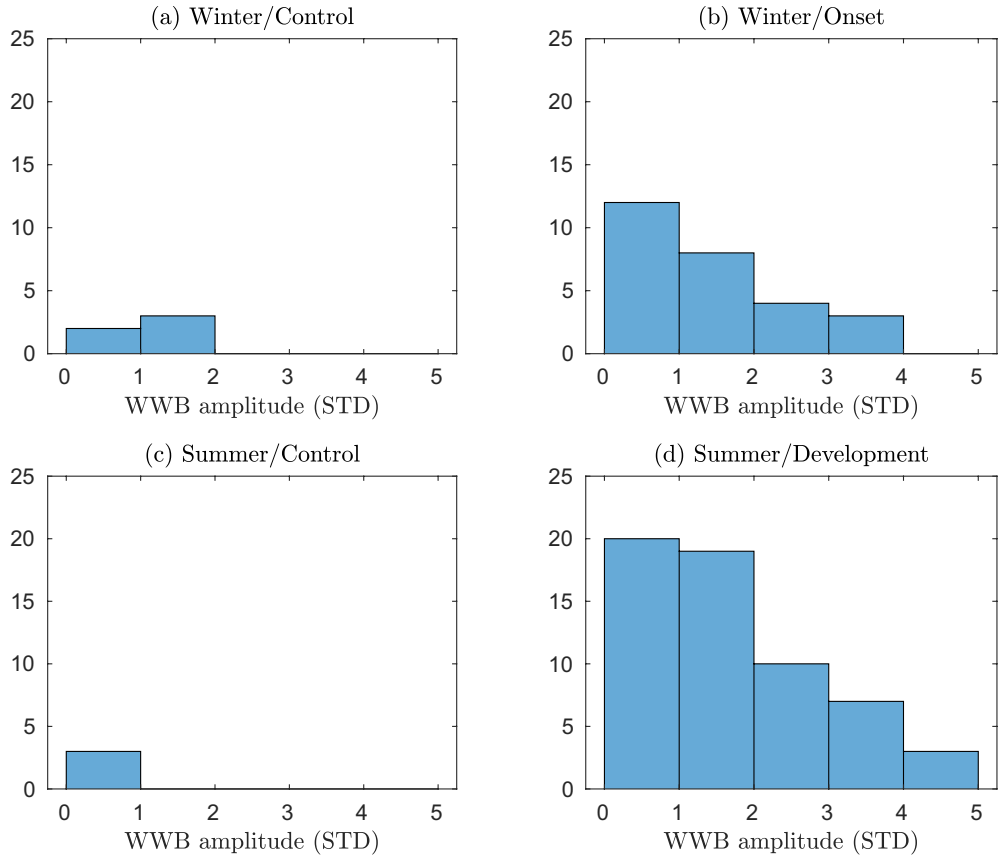

Figure 4. Histograms showing the distribution of WWB amplitude for wind bursts between December and April in the (a) Control and (b) Onset experiments; and between May and November in the (c) Control and (d) Development experiments. Both the frequency and magnitude of WWBs increase dramatically in the perturbation experiments. 1STD = 476 m/s × degree × day, which is the standard deviation of Amp_{WWB} for all simulated WWBs in the three sets of ensemble experiments. This unit is obtained by integrating wind speed anomalies over longitude and time, which gives an integral measure of WWB strength. The results in each panel are based on 18 seasons as each experiment has six ensemble members lasting 3 years each. WWB, westerly wind burst.

in Wheeler and Hendon (2004). In the Development experiment, a significant enhancement of precipitation and westerly wind anomalies occurs along the equator, while the precipitation anomaly in the north western Pacific weakens (Figure 5a).

Computing the difference of the composite MJO between the Development and Control experiments shows a northwest-southeast dipole structure (Figure 5c), suggesting that the imposed SST anomaly in the central-eastern equatorial Pacific during the extended summer enhances the MJO-related convection and westerlies on the equator while reducing convection in the north western Pacific. This creates favorable conditions for WWB generation along the equator and, in a coupled system, would contribute to El Niño growth through the Bjerknes (1969) feedback. Whereas only three WWBs are generated in all 18 years of the Control experiment during the extended summer (1 by the MJO), 59 WWBs are generated in the Development experiment (28 by the MJO) during the same season. On average, the latter implies ~3 WWBs per summer season per year of El Niño development (Figures 4c and 4d).

Out of the 36 selected MJO events in the extended summer in the Development experiment, 26 are wMJO events and 10 are nwMJO events. Thus, compared to the fraction of wMJO events in the Onset experiment (50%), the MJO is significantly more likely to generate WWBs in the Development experiment (72%). These two numbers should be further compared to mere 11% and 3% of wMJO events in the extended winter and summer of the Control experiment, respectively. It is noteworthy that the state dependence of WWBs on SST is most pronounced in our experiments during the development stage of El Niño, which agrees with

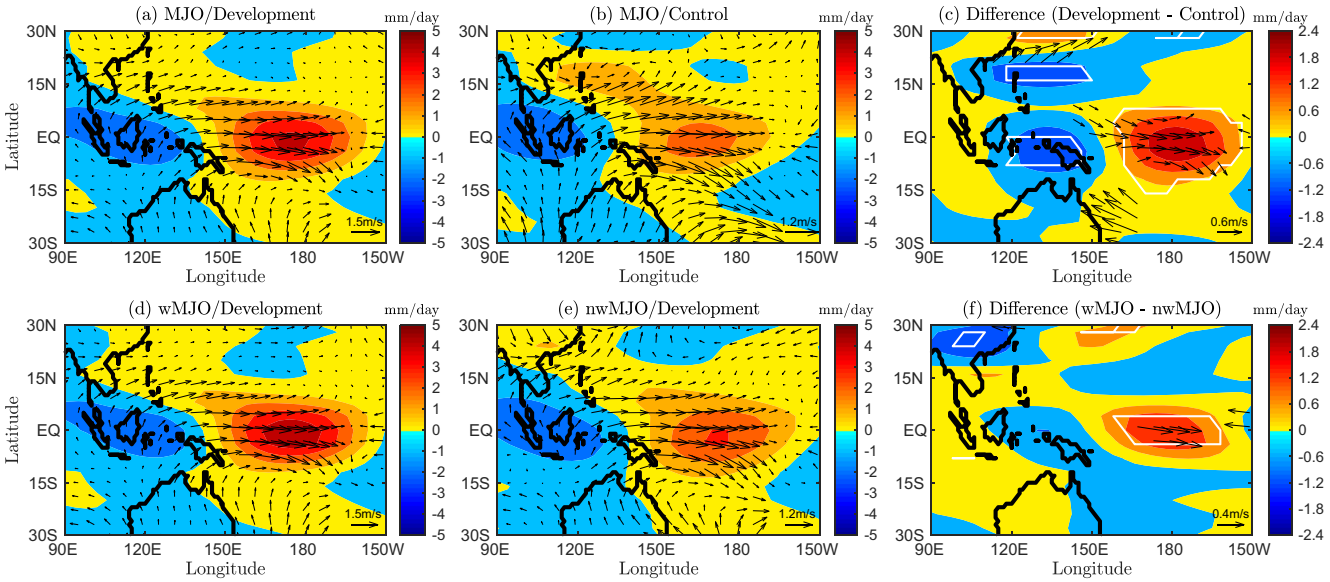

Figure 5. (a)–(c) As in Figure 3 (top row) but for the strongest MJO events simulated between May and November in the (a) Development and (b) Control experiments (36 events are selected in each experiment). (d)–(f) As in Figure 3 (bottom row) but based on (d) 26 wMJO events and (e) 10 nwMJO events identified among the 36 MJO events selected in the Development experiment. MJO, Madden-Julian Oscillation.

the observational analysis of Liang and Fedorov (2021), however, in part this may be due to the larger magnitude and spatial scale of the imposed SST anomaly.

Note that the top 36 MJO events in the Development experiment are significantly stronger than those in the Control experiment (Figures S3c and S3d), therefore overall we would see a greater number of MJO events generated during El Niño development if one defines MJO events based on filtered precipitation averaged over the western-central equatorial Pacific and a fixed threshold.

The composites of space-time filtered precipitation and surface wind anomalies in the Development experiment for wMJO and nwMJO events on $day_{westerly}$ are shown in Figures 5d and 5e. Computing the difference between the two shows a mean enhancement of precipitation in both the central equatorial and western north Pacific, and significantly stronger westerly wind anomalies along the equator (Figure 5f), which is distinct from the dipole structure in Figure 5c. Thus, even though WWBs are more dependent on background conditions during the development stage of El Niño, the MJO internal variability still affects WWBs, with stronger MJO events more likely to generate wind bursts. Figure s6 shows several snapshots of the wMJO event that caused the second WWB in Figure 2c, which highlights how westerly wind anomalies induced by an MJO event with embedded twin tropical cyclones can generate WWBs.

4. Summary and Discussion

Using a novel LAM, which simulates a realistic MJO and WWBs, we examine the response of the MJO to two types of SST anomalies, resembling those observed during the onset and development stages of El Niño, and investigate WWB generation. We pay particular attention to changes to the MJO horizontal structure, which have been overlooked by previous studies. In our Control experiment, forced with monthly climatological SST, only a small number of WWBs are generated. In contrast, adding equatorial SST anomalies during the extended winter and summer seasons greatly enhances WWB generation, increasing the number of WWBs generated by the MJO as a result of the equatorward shift of MJO convective activity.

Specifically, in the Onset experiment, a positive Gaussian-shape SST anomaly with a 1°C maximum temperature is added to the western-central equatorial Pacific during the extended winter (December–April), while westerly wind anomalies (~2 m/s) develop to the west of it. These changes draw MJO convective activity toward the equator, causing the enhancement of convection and westerlies along the equator and a reduction off the equator. The change to the MJO horizontal structure provides more favorable conditions

for WWB generation with about 50% of the MJO events generating WWBs (vs. 11% in the Control). MJO events that generate WWBs have a larger amplitude on average. The average amplitude of the MJO in the extended winter of the Control experiment is comparable to the Onset experiment; therefore, the model enhancement of MJO activity in the equatorial band (5°N–5°S) in boreal spring at the onset of El Niño (also observed in Hendon et al. [2007]) is mostly caused by the induced change in the MJO horizontal structure, consistent with the observational analysis of Liang and Fedorov (2021).

In the Development experiment, a positive Gaussian-shape SST anomaly with a 1.5°C maximum temperature is added to the central-eastern equatorial Pacific during the extended summer (May–November), causing the development of background westerly wind anomalies (~2 m/s) to its west. These changes strengthen MJO activity in the central equatorial Pacific while weaken it in the north western Pacific. The enhanced convection and westerly winds of the MJO near the equator contribute to WWB generation, with more than 70% of MJO events generating WWBs (vs. 3% in the Control). This suggests WWBs are more SST-dependent during the development stage of El Niño than during the onset stage, but this may be due in part to a larger magnitude and spatial scale of the emerging SST anomalies. Compared to MJO events that fail to generate WWBs, events that do have larger amplitudes on average.

While relatively simple, our experiments enable us to disentangle the complex interactions involving the MJO, WWBs and SST. Together with the companion observational study (Liang & Fedorov, 2021), this study clearly illustrates the mechanism by which WWB generation is enhanced by equatorial SST anomalies modifying MJO convective activity. Our experiments further suggest that WWBs behave as an SST-dependent multiplicative noise both during the onset and development stages of El Niño, although the link to SST is stronger during the development stage. Yet, even with favorable background SST anomalies on the equator, WWB generation shows strong variability across different MJO events.

Data Availability Statement

LAM simulation output is archived in Dryad Digital Repository and can be downloaded from https://doi.org/10.5061/dryad.d51c5b010.

Acknowledgments
This study was supported by grants to Alexey Fedorov from NSF (AGS-1405272), NASA (NNX17AH21G), and NOAA (NA20OAR4310377). Patrick Haertel was supported by NSF Grant 1561066. The authors thank two anonymous reviewers for their constructive comments and suggestions, which improved the quality of the manuscript.

References

Andersen, J. A., & Kuang, Z. (2012). Moist static energy budget of MJO-like disturbances in the atmosphere of a zonally symmetric aquaplanet. *Journal of Climate*, *25*(8), 2782–2804. https://doi.org/10.1175/jcli-d-11-00168.1

Ashok, K., Behera, S. K., Rao, S. A., Weng, H., & Yamagata, T. (2007). El Niño Modoki and its possible teleconnection. *Journal of Geophysical Research: Oceans*, *112*(C11). https://doi.org/10.1029/2006jc003798

Bjerknes, J. (1969). Atmospheric teleconnections from the equatorial pacific1. *Monthly Weather Review*, *97*(3), 163–172. https://doi.org/10.1175/1520-0493(1969)097<0163:atftep>2.3.co;2

Capotondi, A., Wittenberg, A. T., Newman, M., Di Lorenzo, E., Yu, J.-Y., Braconnot, P., et al. (2015). Understanding ENSO diversity. *Bulletin of the American Meteorological Society*, *96*(6), 921–938. https://doi.org/10.1175/bams-d-13-00117.1

Chen, X., Ling, J., & Li, C. (2016). Evolution of the Madden-Julian Oscillation in two types of El Niño. *Journal of Climate*, *29*(5), 1919–1934. https://doi.org/10.1175/jcli-d-15-0486.1

Chu, P.-S. (1988). Extratropical forcing and the burst of equatorial westerlies in the western Pacific: A synoptic study. *Journal of the Meteorological Society of Japan*, *66*(4), 549–564. https://doi.org/10.2151/jmsj1965.66.4_549

Dee, D. P., Uppala, S. M., Simmons, A. J., Berrisford, P., Poli, P., Kobayashi, S., et al. (2011). The ERA-interim reanalysis: Configuration and performance of the data assimilation system. *Quarterly Journal of the Royal Meteorological Society*, *137*(656), 553–597. https://doi.org/10.1002/qj.828

Eisenman, I., Yu, L., & Tziperman, E. (2005). Westerly wind bursts: ENSO's tail rather than the dog?. *Journal of Climate*, *18*(24), 5224–5238. https://doi.org/10.1175/jcli3588.1

Fedorov, A. V. (2002). The response of the coupled tropical ocean-atmosphere to westerly wind bursts. *Quarterly Journal of the Royal Meteorological Society*, *128*(579), 1–23. https://doi.org/10.1002/qj.200212857901

Fedorov, A. V., Harper, S. L., Philander, S. G., Winter, B., & Wittenberg, A. (2003). How predictable is El Niño? *Bulletin of the American Meteorological Society*, *84*(7), 911–920. https://doi.org/10.1175/bams-84-7-911

Fedorov, A. V., Hu, S., Lengaigne, M., & Guilyardi, E. (2015). The impact of westerly wind bursts and ocean initial state on the development, and diversity of El Niño events. *Climate Dynamics*, *44*(5–6), 1381–1401. https://doi.org/10.1007/s00382-014-2126-4

Gebbie, G., Eisenman, I., Wittenberg, A., & Tziperman, E. (2007). Modulation of westerly wind bursts by sea surface temperature: A semistochastic feedback for ENSO. *Journal of the Atmospheric Sciences*, *64*(9), 3281–3295. https://doi.org/10.1175/jas4029.1

Gebbie, G., & Tziperman, E. (2009). Predictability of SST-modulated westerly wind bursts. *Journal of Climate*, *22*(14), 3894–3909. https://doi.org/10.1175/2009jcli2516.1

Gill, A. E. (1980). Some simple solutions for heat-induced tropical circulation. *Quarterly Journal of the Royal Meteorological Society*, *106*(449), 447–462. https://doi.org/10.1002/qj.49710644905

Gushchina, D., & Dewitte, B. (2012). Intraseasonal tropical atmospheric variability associated with the two flavors of El Niño. *Monthly Weather Review*, *140*(11), 3669–3681. https://doi.org/10.1175/mwr-d-11-00267.1

Haertel, P. T. (2012). A Lagrangian method for simulating geophysical fluids. *Lagrangian Modeling of the Atmosphere*, 85–98.American Geophysical Union.
Haertel, P. T. (2018). Sensitivity of the Madden Julian Oscillation to ocean warming in a Lagrangian atmospheric model. *Climate*, *6*(2), 45. https://doi.org/10.3390/cli6020045
Haertel, P. T. (2020). Prospects for erratic and intensifying Madden-Julian oscillations. *Climate*, *8*(2), 24. https://doi.org/10.3390/cli8020024
Haertel, P. T., Boos, W., & Straub, K. (2017). Origins of moist air in global Lagrangian simulations of the Madden–Julian Oscillation. *Atmosphere*, *8*(9), 158. https://doi.org/10.3390/atmos8090158
Haertel, P. T., Kiladis, G. N., Denno, A., & Rickenbach, T. M. (2008). Vertical-mode decompositions of 2-day waves and the Madden-Julian Oscillation. *Journal of the Atmospheric Sciences*, *65*(3), 813–833. https://doi.org/10.1175/2007jas2314.1
Haertel, P. T., Straub, K., & Budsock, A. (2015). Transforming circumnavigating Kelvin waves that initiate and dissipate the Madden-Julian Oscillation. *Quarterly Journal of the Royal Meteorological Society*, *141*(690), 1586–1602. https://doi.org/10.1002/qj.2461
Haertel, P. T., Straub, K., & Fedorov, A. (2014). Lagrangian overturning and the Madden-Julian Oscillation. *Quarterly Journal of the Royal Meteorological Society*, *140*(681), 1344–1361. https://doi.org/10.1002/qj.2216
Hartten, L. M. (1996). Synoptic settings of westerly wind bursts. *Journal of Geophysical Research*, *101*(D12), 16997–17019. https://doi.org/10.1029/96jd00030
Hendon, H. H., & Liebmann, B. (1990). The intraseasonal (30-50 day) oscillation of the Australian summer monsoon. *Journal of the Atmospheric Sciences*, *47*(24), 2909–2924. https://doi.org/10.1175/1520-0469(1990)047<2909:tidoot>2.0.co;2
Hendon, H. H., Wheeler, M. C., & Zhang, C. (2007). Seasonal dependence of the MJO-ENSO relationship. *Journal of Climate*, *20*(3), 531–543. https://doi.org/10.1175/jcli4003.1
Hendon, H. H., Zhang, C., & Glick, J. D. (1999). Interannual variation of the Madden-Julian Oscillation during austral summer. *Journal of Climate*, *12*(8), 2538–2550. https://doi.org/10.1175/1520-0442(1999)012<2538:ivotmj>2.0.co;2
Hirst, A. C. (1986). Unstable and damped equatorial modes in simple coupled ocean-atmosphere models. *Journal of the Atmospheric Sciences*, *43*(6), 606–632. https://doi.org/10.1175/1520-0469(1986)043<0606:uademi>2.0.co;2
Hu, S., & Fedorov, A. V. (2018). Cross-equatorial winds control El Niño diversity and change. *Nature Climate Change*, *8*(9), 798–802. https://doi.org/10.1038/s41558-018-0248-0
Hu, S., & Fedorov, A. V. (2019). The extreme El Niño of 2015-2016: The role of westerly and easterly wind bursts, and preconditioning by the failed 2014 event. *Climate Dynamics*, *52*(12), 7339–7357. https://doi.org/10.1007/s00382-017-3531-2
Hu, S., Fedorov, A. V., Lengaigne, M., & Guilyardi, E. (2014). The impact of westerly wind bursts on the diversity and predictability of El Niño events: An ocean energetics perspective. *Geophysical Research Letters*, *41*(13), 4654–4663. https://doi.org/10.1002/2014gl059573
Hung, M.-P., Lin, J.-L., Wang, W., Kim, D., Shinoda, T., & Weaver, S. J. (2013). MJO and convectively coupled equatorial waves simulated by CMIP5 climate models. *Journal of Climate*, *26*(17), 6185–6214. https://doi.org/10.1175/jcli-d-12-00541.1
Kao, H.-Y., & Yu, J.-Y. (2009). Contrasting eastern-Pacific and central-Pacific types of ENSO. *Journal of Climate*, *22*(3), 615–632. https://doi.org/10.1175/2008jcli2309.1
Kessler, W. S. (2001). EOF representations of the Madden-Julian Oscillation and its connection with ENSO. *Journal of Climate*, *14*(13), 3055–3061. https://doi.org/10.1175/1520-0442(2001)014<3055:erotmj>2.0.co;2
Kessler, W. S., & Kleeman, R. (2000). Rectification of the Madden-Julian Oscillation into the ENSO cycle. *Journal of Climate*, *13*(20), 3560–3575. https://doi.org/10.1175/1520-0442(2000)013<3560:rotmjo>2.0.co;2
Kessler, W. S., McPhaden, M. J., & Weickmann, K. M. (1995). Forcing of intraseasonal kelvin waves in the equatorial pacific. *Journal of Geophysical Research*, *100*(C6), 10613–10631. https://doi.org/10.1029/95jc00382
Kug, J.-S., Jin, F.-F., & An, S.-I. (2009). Two types of El Niño events: Cold tongue El Niño and warm pool El Niño. *Journal of Climate*, *22*(6), 1499–1515. https://doi.org/10.1175/2008jcli2624.1
Lau, K.-M., & Chan, P. H. (1986). Aspects of the 40-50 day oscillation during the northern summer as inferred from outgoing longwave radiation. *Monthly Weather Review*, *114*(7), 1354–1367. https://doi.org/10.1175/1520-0493(1986)114<1354:aotdod>2.0.co;2
Lengaigne, M., Boulanger, J.-P., Menkes, C., Madec, G., Delecluse, P., Guilyardi, E., & Slingo, J. (2003). The March 1997 westerly wind event and the onset of the 1997/98 El Niño: Understanding the role of the atmospheric response. *Journal of Climate*, *16*(20), 3330–3343. https://doi.org/10.1175/1520-0442(2003)016<3330:tmwwea>2.0.co;2
Lengaigne, M., Boulanger, J.-P., Menkes, C., Masson, S., Madec, G., & Delecluse, P. (2002). Ocean response to the march 1997 westerly wind event. *Journal of Geophysical Research: Oceans*, *107*(C12). SRF-16. https://doi.org/10.1029/2001jc000841
Lian, T., Chen, D., Tang, Y., Liu, X., Feng, J., & Zhou, L. (2018). Linkage between westerly wind bursts and tropical cyclones. *Geophysical Research Letters*, *45*(20), 11–431. https://doi.org/10.1029/2018gl079745
Liang, Y., & Fedorov, A. V. (2021). Linking the Madden-Julian Oscillation, tropical cyclones and westerly wind bursts as part of El Niño development. *Climate Dynamics*. https://doi.org/10.1007/s00382-021-05757-1
Liebmann, B., Hendon, H. H., & Glick, J. D. (1994). The relationship between tropical cyclones of the western Pacific and Indian oceans and the Madden-Julian Oscillation. *Journal of the Meteorological Society of Japan*, *72*(3), 401–412. https://doi.org/10.2151/jmsj1965.72.3_401
Madden, R. A., & Julian, P. R. (1972). Description of global-scale circulation cells in the tropics with a 40-50 day period. *Journal of the Atmospheric Sciences*, *29*(6), 1109–1123. https://doi.org/10.1175/1520-0469(1972)029<1109:dogscc>2.0.co;2
Matsuno, T. (1966). Quasi-geostrophic motions in the equatorial area. *Journal of the Meteorological Society of Japan*, *44*(1), 25–43. https://doi.org/10.2151/jmsj1965.44.1_25
McPhaden, M. J., & Yu, X. (1999). Equatorial waves and the 1997-98 El Niño. *Geophysical Research Letters*, *26*(19), 2961–2964. https://doi.org/10.1029/1999gl004901
Neelin, J. D., Jin, F.-F., & Syu, H.-H. (2000). Variations in ENSO phase locking. *Journal of Climate*, *13*(14), 2570–2590. https://doi.org/10.1175/1520-0442(2000)013<2570:viepl>2.0.co;2
Puy, M., Vialard, J., Lengaigne, M., & Guilyardi, E. (2016). Modulation of equatorial Pacific westerly/easterly wind events by the Madden–Julian Oscillation and convectively-coupled Rossby waves. *Climate Dynamics*, *46*(7–8), 2155–2178. https://doi.org/10.1007/s00382-015-2695-x
Rasmusson, E. M., & Carpenter, T. H. (1982). Variations in tropical sea surface temperature and surface wind fields associated with the southern oscillation/El Niño. *Monthly Weather Review*, *110*(5), 354–384. https://doi.org/10.1175/1520-0493(1982)110<0354:vitsst>2.0.co;2
Seiki, A., & Takayabu, Y. N. (2007). Westerly wind bursts and their relationship with intraseasonal variations and ENSO. Part I: Statistics. *Monthly Weather Review*, *135*(10), 3325–3345. https://doi.org/10.1175/mwr3477.1
Seiki, A., Takayabu, Y. N., Yasuda, T., Sato, N., Takahashi, C., Yoneyama, K., & Shirooka, R. (2011). Westerly wind bursts and their relationship with ENSO in CMIP3 models. *Journal of Geophysical Research: Atmospheres*, *116*(D3). https://doi.org/10.1029/2010jd015039

Slingo, J., Rowell, D., Sperber, K., & Nortley, F. (1999). On the predictability of the interannual behaviour of the Madden-Julian Oscillation and its relationship with El Niño. *Quarterly Journal of the Royal Meteorological Society*, *125*(554), 583–609. https://doi.org/10.1256/smsqj.55410

Tziperman, E., & Yu, L. (2007). Quantifying the dependence of westerly wind bursts on the large-scale tropical pacific SST. *Journal of Climate*, *20*(12), 2760–2768. https://doi.org/10.1175/jcli4138a.1

Vecchi, G. A., & Harrison, D. E. (2000). Tropical Pacific sea surface temperature anomalies, El Niño, and equatorial westerly wind events. *Journal of Climate*, *13*(11), 1814–1830. https://doi.org/10.1175/1520-0442(2000)013<1814:tpssta>2.0.co;2

Wheeler, M., & Kiladis, G. N. (1999). Convectively coupled equatorial waves: Analysis of clouds and temperature in the wavenumber-frequency domain. *Journal of the Atmospheric Sciences*, *56*(3), 374–399. https://doi.org/10.1175/1520-0469(1999)056<0374:ccewao>2.0.co;2

Wheeler, M. C., & Hendon, H. H. (2004). An all-season real-time multivariate MJO index: Development of an index for monitoring and prediction. *Monthly Weather Review*, *132*(8), 1917–1932. https://doi.org/10.1175/1520-0493(2004)132<1917:aarmmi>2.0.co;2

Yeh, S.-W., Kug, J.-S., Dewitte, B., Kwon, M.-H., Kirtman, B. P., & Jin, F.-F. (2009). El Niño in a changing climate. *Nature*, *461*(7263), 511–514. https://doi.org/10.1038/nature08316

Yu, S., & Fedorov, A. V. (2020). The role of westerly wind bursts during different seasons versus ocean heat recharge in the development of extreme El Niño in a climate model. *Geophysical Research Letters*, e2020GL088381.

Zhang, C., & Dong, M. (2004). Seasonality in the Madden-Julian Oscillation. *Journal of Climate*, *17*(16), 3169–3180. https://doi.org/10.1175/1520-0442(2004)017<3169:sitmo>2.0.co;2